Effect of phonon anharmonicity on ferroelectricity in $Eu_xBa_{1-x}TiO_3$

Bommareddy Poojitha,[1] Km Rubi,[2] Soumya Sarkar,[3,4] R. Mahendiran,[2,3,*] T. Venkatesan,[2,3,4,*] and Surajit Saha[1,*]

[1]*Department of Physics, Indian Institute of Science Education and Research, Bhopal 462066, India*

[2]*Department of Physics, National University of Singapore, Singapore 117551, Singapore*

[3]*NUSNNI-NanoCore, National University of Singapore, Singapore 117411, Singapore*

[4]*NUS Graduate School for Integrative Sciences and Engineering, Singapore 117456, Singapore*

(Received 3 January 2019; revised manuscript received 6 February 2019; published 28 February 2019)

Investigating the competition between ferroelectric ordering and quantum fluctuations is essential for tailoring the desired functionalities of mixed ferroelectric and incipient ferroelectric systems, like, $(Ba, Sr)TiO_3$ and $(Eu, Ba)TiO_3$. Recently, it has been shown that suppression of quantum fluctuations increases ferroelectric ordering in $(Eu, Ba)TiO_3$ and since these phenomena are coupled to crystallographic phase transitions it is essential to understand the role of phonons. Here, we observe that the unusual temperature dependence of phonons in $BaTiO_3$ gets suppressed when Ba^{2+} is replaced by Eu^{2+}. This manifests in a decrease in the cubic-to-tetragonal (i.e., para-to-ferroelectric) phase transition temperature (by 150 K) and a complete suppression of tetragonality of the lattice (at room temperature by 40% replacement of Ba^{2+} by Eu^{2+}). We have quantified the anharmonicity of the phonons and observed that the replacement of Ba^{2+} by Eu^{2+} suppresses it (by 93%) with a resultant lowering of the ferroelectric ordering temperature in the $Eu_xBa_{1-x}TiO_3$. This suggests that tuning phonon anharmonicity can be an important route to ferroelectric materials.

DOI: 10.1103/PhysRevMaterials.3.024412

I. INTRODUCTION

Ferroelectric materials are characterized by features like spontaneous polarization, nonlinear dielectric behavior, large electro-optic coefficient, high permittivity, as well as pyroelectric and piezoelectric properties, making it possible to design various functional devices out of these materials [1]. One of the most studied ferroelectric materials with perovskite structure is $BaTiO_3$, which also exhibits a rich variety of structural phases. $BaTiO_3$ undergoes a series of structural transitions with increasing temperature [2], showing a low temperature rhombohedral to orthorhombic phase transition at around 193 K. This is followed by an orthorhombic to tetragonal phase change at around 280 K and then a tetragonal to cubic transition at around 395 K. $BaTiO_3$ is paraelectric in the high temperature cubic phase. However, in the low temperature phases it becomes a ferroelectric as the macroscopic electric polarization aligns in parallel to [001], [011], and [111] axes (denoted in terms of cubic notation) of the thermally induced crystallographic phases characterized by tetragonal, orthorhombic, and rhombohedral unit cell, respectively [2]. On the contrary, $EuTiO_3$ (also a perovskite) is an incipient ferroelectric where there exists a competition between the ferroelectric order parameter and quantum fluctuations [3,4]. Though $EuTiO_3$ has a soft polar phonon mode, the polarization does not freeze down to the lowest temperature due to quantum fluctuations [4]. Further, unlike the other similar incipient ferroelectrics, e.g., $SrTiO_3$ and $KTaO_3$, $EuTiO_3$ undergoes a paramagnetic to *G*-type antiferromagnetic transition below about 5 K due to its localized $4f$ electrons ($S = 7/2$) [5] and exhibits a giant magnetodielectric effect [3,4].

Inducing ferroelectric ordering in incipient ferroelectrics has been of great importance not only being fundamentally interesting but also because it is important for realizing their technological potentials. Introduction of Ba^{2+} in $SrTiO_3$ and Nb^{5+} in $KTaO_3$ have been known to induce ferroelectric ordering [6–8]. Recently, it was demonstrated that by doping Ba^{2+} in $EuTiO_3$ one could suppress the quantum fluctuations in $EuTiO_3$, thereby inducing ferroelectric ordering [9]. Besides the suppression of quantum fluctuations, magnetoelectric effects have also been observed in Ba^{2+} doped $EuTiO_3$ [3,10,11]. Moreover, $(Eu, Ba)TiO_3$ has been proposed as a model system to search for electron electric dipole moment, which is of vital importance to study charge-parity violation [12].

Phonons have an intimate relationship with ferroelectric ordering in $BaTiO_3$ and so should be the case in the incipient ferroelectric $EuTiO_3$ upon doping Ba^{2+}. However, the exact mechanism by which phonons play a role in this competition between ferroelectric ordering and quantum fluctuations remains unclear. Notably, in such incipient ferroelectrics (like $EuTiO_3$, $SrTiO_3$, etc.) the phase transitions are coupled to lattice, causing these materials to exhibit quantum criticality over a wide range of temperatures [13]. At such finite temperatures phonon anharmonicity (i.e., phonon-phonon scattering) becomes crucial for understanding the ground state of the incipient ferroelectrics [3,14]. In this article, we investigate the phonons anharmonicities in $BaTiO_3$ as a function of Eu^{2+} doping in order to establish the correlation between anharmonicity and ferroelectric ordering in the $Eu_xBa_{1-x}TiO_3$ systems.

*Authors to whom correspondence should be addressed: phyrm@nus.edu.sg; venky@nus.edu.sg; surajit@iiserb.ac.in

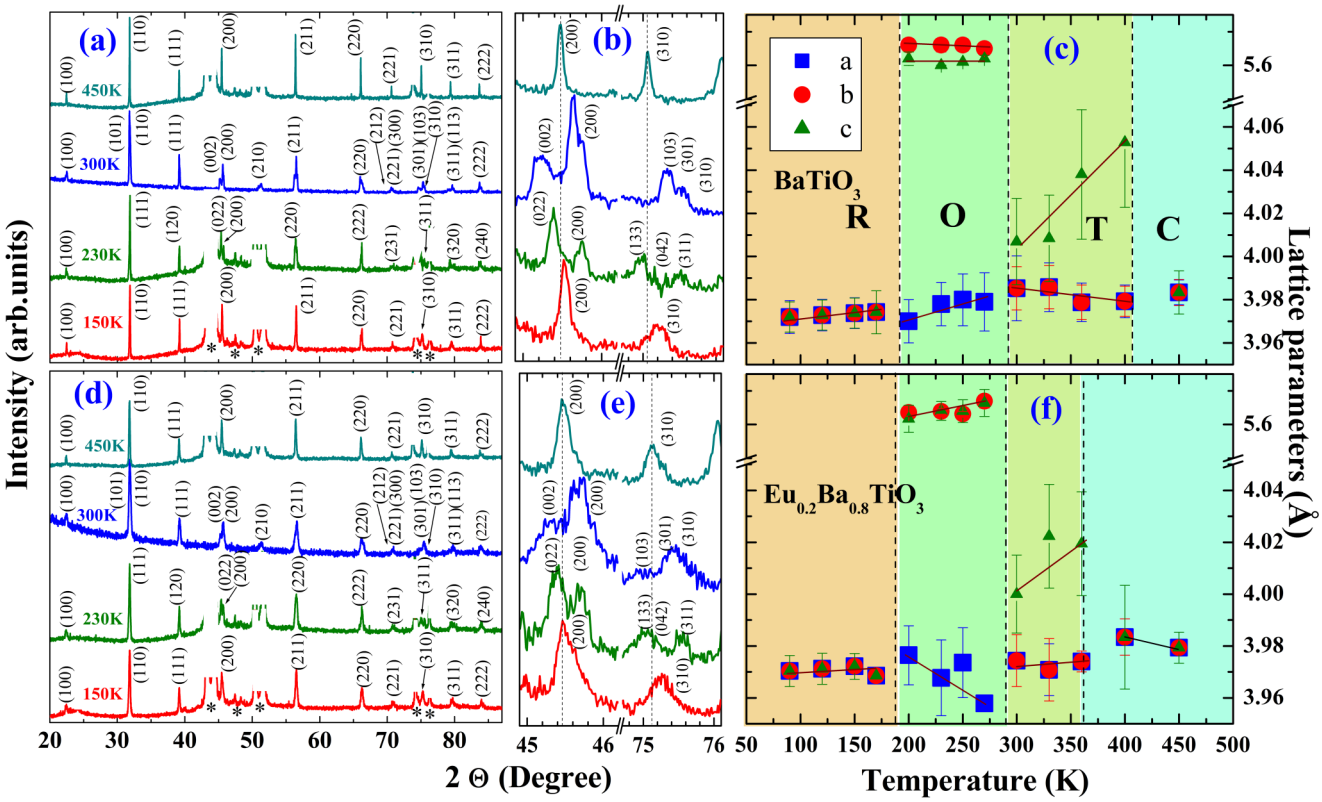

FIG. 1. X-ray diffraction patterns of $BaTiO_3$ (a), (b) and $Eu_{0.2}Ba_{0.8}TiO_3$ (d), (e) at various temperatures with corresponding (*hkl*) values. The middle column (b), (e) shows the specific reflection peaks that correspond to the structural phase transitions. The right column shows the lattice parameters of (c) $BaTiO_3$ and (f) $Eu_{0.2}Ba_{0.8}TiO_3$ as a function of temperature as it undergoes the structural phase transitions (from R = Rhombohedral to O = Orthorhombic to T = Tetragonal to C = Cubic phases shown by the shaded regions). The solid lines in (c) and (f) are guides to the eye. The additional peaks marked with asterisk (*) symbols in the regions between 40 and 55° and near 75° in (a) and (d) are due to the low temperature sample stage (LTStage) that have been partly removed from the data for clarity. The room temperature (300 K) data do not have these additional peaks and hence the (210) sample peak is clearly visible.

II. RESULTS AND DISCUSSION

Structure and phase purity of $Eu_xBa_{1-x}TiO_3$. Polycrystalline $BaTiO_3$ and $Eu_xBa_{1-x}TiO_3$ ($x = 0.1, 0.2, 0.3, 0.4$, and 1) powder samples were synthesized using a solid state reaction route (see Sec. III) and are found to be in a highly pure phase (see Sec. S1 and Figs. S1–S3 in the Supplemental Material for details [15]). The rich variety of structural phases exhibited by these samples have been captured in the temperature-dependent x-ray diffraction patterns, shown in Fig. 1. Figure 1(c) shows the changes in the lattice parameters as a function of temperature in the four different structural phases [16]. A partial replacement of Ba^{2+} by Eu^{2+} (such as in $Eu_{0.2}Ba_{0.8}TiO_3$) reduces the lattice parameters as shown in Fig. 1(f) (and Fig. S2 in the Supplemental Material [15]) and lowers the cubic-to-tetragonal phase transition temperature. However, no significant change in the transition temperatures of the low temperature phases could be detected with Eu^{2+} doping. The reason is not clear at present. However, as the para-to-ferroelectric phase transition is specifically associated with the cubic-to-tetragonal structural change, our emphasis in this article will be on this crystallographic phase transition.

Γ*-point Raman phonons of* $Eu_xBa_{1-x}TiO_3$. The ferroelectric transition in $BaTiO_3$ is ferrodistortive in nature. Therefore, in both the ferro- and paraelectric phases it has one formula unit (5 atoms) per unit cell that gives rise to 12 optical phonon modes at the Γ point of the Brillouin zone. In the paraelectric-cubic phase none of the phonons ($3F_{1u} + F_{2u}$) are Raman active whereas in the ferroelectric-tetragonal phase there are $3A_1$, B_1, and $4E$ Raman modes. A detailed description of the origin of these Raman modes at the Γ point are provided in the Supplemental Material (Sec. S2) [15]. Figures 2(a) and 2(b) show the typical Raman spectra presenting the prominent phonon modes of $BaTiO_3$ and $Eu_{0.2}Ba_{0.8}TiO_3$ at 78 K (obtained via Lorentz spectral fitting). The observed mode frequencies and their assignments based on previous reports [17–22] are listed in Table I. As can be seen in Table I, the prominent modes near 265 cm^{-1} (*P5*) and 520 cm^{-1} (*P8*) undergo a *redshift* upon Eu^{2+} incorporation that can be attributed to an increase in the atomic mass while the *P6* mode at 308 cm^{-1} does not respond to the change in atomic mass because Ba/Eu atoms are not involved in this vibration [22]. Figure S4 (Supplemental Material [15]) shows the dependence of the Raman spectrum at 300 K as a function of Eu^{2+} incorporation by replacing Ba^{2+} in $BaTiO_3$. The absence of the 308 cm^{-1} (*P6*) mode for 40% doping of Eu^{2+} in $BaTiO_3$ (i.e., $Eu_{0.4}Ba_{0.6}TiO_3$) and above suggests that its crystal structure is not tetragonal at 300 K [17,19,21–24] and, therefore, it is no longer a room temperature ferroelectric.

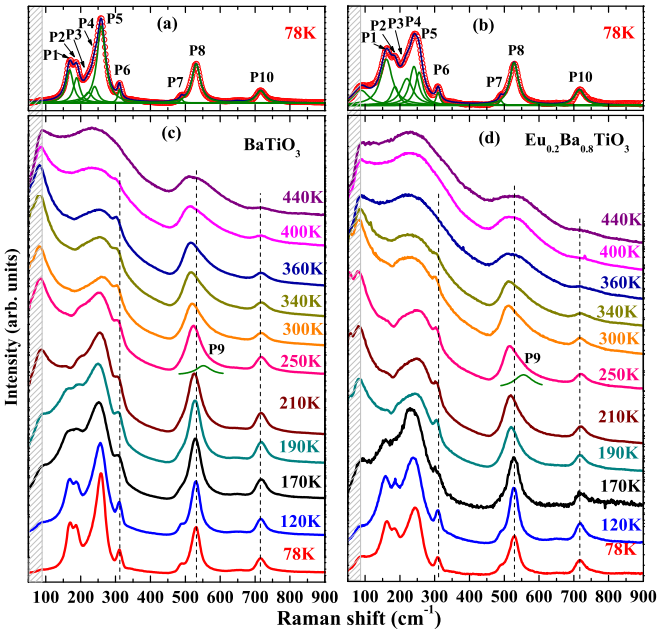

FIG. 2. Raman spectra of $BaTiO_3$ and $Eu_{0.2}Ba_{0.8}TiO_3$ at a few typical temperatures showing the evolution of the phonon modes with temperature. The shading indicates the region affected by the optical band-pass filter as discussed in the text. The spectra have been analyzed using Lorentz functions to identify the phonon modes *P1* to *P10* (shown in green) in (a) and (b). The mode *P9* [shown in green in (c) and (d)] is present above ∼190 K in the orthorhombic and tetragonal phases.

Notably, the other modes show a small or almost no shift in phonon frequency at room temperature upon Eu incorporation implying that there is indirect or no involvement of Ba/Eu atoms in these vibrations. However, as shown by Freire and Katiyar [22] in their lattice dynamical calculations (LDC), all the vibrations at the Γ point involve all three atoms (Ba, Ti, O) except the B_1 mode at 308 cm^{-1}. Our data at room temperature, therefore, corroborate with the LDC for the prominent modes at 265 (A_1), 308 (B_1), and 520 (A_1) cm^{-1}. However, the corresponding redshift for the other modes due to Eu incorporation is not observed, which is highly unusual. In order to understand this phenomenon, we have performed a temperature-dependent study which is discussed below. The shaded region of the spectra below 100 cm^{-1} is influenced by the cutoff of the band-pass filter used during the measurements and, hence, will not be used for drawing any conclusion.

Figures 2(c) and 2(d) show the temperature-dependent Raman spectra of $BaTiO_3$ and $Eu_{0.2}Ba_{0.8}TiO_3$ to emphasize the effect of structural changes on the Raman spectrum (temperature dependence of the Raman spectra of $Eu_xBa_{1-x}TiO_3$ for $x = 0.1, 0.3, 0.4$, and 1 are shown in Figs. S5 and S6 in the Supplemental Material [15]). For $BaTiO_3$, it may be noted that as the temperature increases there is a clear and systematic rise in the background spectral line shape below 200 cm^{-1}. Such a line shape at lower frequencies has been reported previously [17,20–22,25–28] and may be attributed to the contribution from the soft $E(TO_1)$ mode at 35 cm^{-1} (not captured in our data due to the cutoff of the band-pass filter) [17,29]. A similar temperature-dependent change in the line shape at lower frequencies can also be seen in $Eu_{0.2}Ba_{0.8}TiO_3$ but occurs at even lower temperatures [Fig. 2(d)], which may be associated with the phonon anharmonicity and a lower unit cell volume of $Eu_{0.2}Ba_{0.8}TiO_3$. Further, mode *P6* at 308 cm^{-1} is representative of the ferroelectric phase of $BaTiO_3$ [17,21–24,26] that can be seen at temperatures below ∼400 K [Fig. 2(c)], whereas this mode in $Eu_{0.2}Ba_{0.8}TiO_3$ is absent above ∼ 360 K [Fig. 2(d)] thus suggesting a lowering of the para-to-ferroelectric transition temperature in $Eu_{0.2}Ba_{0.8}TiO_3$. The most noticeable changes in the spectra (of both $BaTiO_3$ and $Eu_{0.2}Ba_{0.8}TiO_3$) with varying temperature occur as a (dis)appearance of phonon modes and unusual / anomalous shift of the modes. In order to quantify these temperature-dependent changes, the spectra at various temperatures have been fitted with Lorentzian functions identifying the various phonons [peaks *P1–P10* shown in Figs. 2(a) and 2(b)] [18,22]. It must be noted that during the spectral fitting we have not considered the coupling of modes with A_1 symmetry as was proposed earlier [25,26] because (a) our samples are polycrystalline powders where disorders are endemic and hence it is difficult to materialize such polariton couplings, and (b) we have not observed a very clear presence of the well-known

TABLE I. Assignment of the Raman active phonon modes (and their frequencies in cm^{-1} unit) of $BaTiO_3$ and $Eu_{0.2}Ba_{0.8}TiO_3$ at 78 K (rhombohedral), 230 K (orthorhombic), and 300 K (tetragonal) obtained by fitting the experimental data.

		$BaTiO_3$			$Eu_{0.2}Ba_{0.8}TiO_3$		
Mode name	Mode symmetry	At 78 K	At 230 K	At 300 K	At 78 K	At 230 K	At 300 K
P1	$A_1(TO_1)$	168	155	Absent	161	154	Absent
P2	$A_1(LO_1)$	188	195	Absent	186	192	Absent
P3	Disorder induced Raman modes[a]	222	218	218	220	209	208
P4		240	Absent	Absent	240	Absent	Absent
P5	$A_1(TO_2)$	259	258	264	255	258	253
P6	B_1	311	309	308	310	307	306
P7	$A_1(LO_2)/E(LO_3)$	489	Absent	Absent	490	Absent	Absent
P8	$E(TO_4)$	531	524	520	528	516	514
P9	$A_1(TO_3)$	Absent	551	556	Absent	555	558
P10	$A_1(LO_3)/E(LO_4)$	716	717	719	716	718	720

[a]The modes *P3* and *P4* are assigned to disorder induced Raman active modes [18].

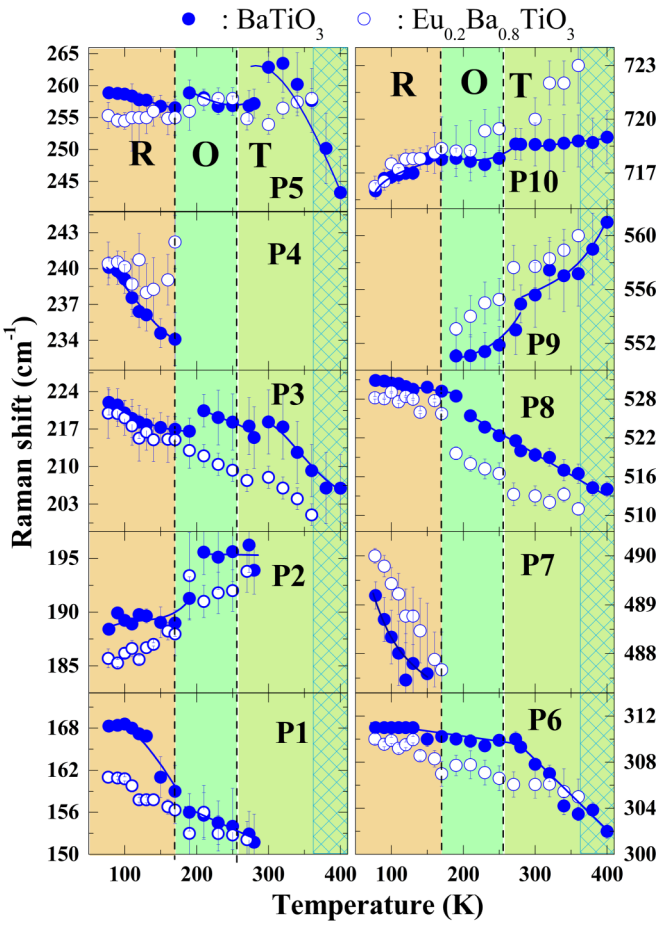

FIG. 3. Frequency of all the phonon modes (*P1* to *P10*) as a function of temperature. All the modes respond to the structural phase transitions as the temperature varies. Effect of Ba^{2+} replacement by Eu^{2+} is also evident in all the modes manifested as the change in phonon anharmonicity, discussed in the text. The color-shaded regions indicate the various structural phases as indicated by the letters R: Rhombohedral, O: Orthorhombic, and T: Tetragonal. The cross-shaded region indicates the Cubic phase for $Eu_{0.2}Ba_{0.8}TiO_3$. The solid lines are guides to the eye.

depolarization dip near 180 cm^{-1} in the tetragonal phase, thus signifying the absence of phonon coupling [26–34]. The temperature dependence of the phonon mode frequency (ω) for both $BaTiO_3$ and $Eu_{0.2}Ba_{0.8}TiO_3$ shows characteristic signatures of the structural phase transitions (see Fig. 3). Notably, peaks *P4* and *P7* near 240 and 489 cm^{-1}, respectively, in $BaTiO_3$ disappear and a new peak (*P9*) appears at 552 cm^{-1} above 190 K owing to the rhombohedral to orthorhombic phase transition. A *jump* [18] in the phonon frequency for the peaks *P3* and *P5* as well as a change in slope (ω vs T) for peaks *P1* and *P8* can be observed across the structural transition. As the temperature increases beyond 280 K, peaks *P1* and *P2* become weak, finally merging with the broad background [that arises from the low frequency $E(TO_1)$ mode]. Peaks *P3* and *P5* show another *jump* in frequency while a change in slope (ω vs T) for *P6* and *P9* can be seen at the same temperature, which can be attributed to the orthorhombic to tetragonal phase transition at ∼280 K. It should be noted that though for most of the peaks the ω shows a decreasing trend with increasing temperature, which is a signature of normal lattice expansion due to quasiharmonic behavior, the peaks *P2*, *P9*, and *P10* show an anomalous trend (an increase in frequency) with temperature. Such an anomaly may arise from strong phonon-phonon anharmonic interactions [35–38], which will be discussed later. The behavior of the respective phonon modes in $Eu_{0.2}Ba_{0.8}TiO_3$, with regard to their appearance/disappearance at crystallographic phase transition temperatures is similar to that in $BaTiO_3$ [see Fig. 2(d)].

Notably, Eu doping also gives rise to two stark differences in the temperature-dependent evolution of the phonon modes in $BaTiO_3$. First, the temperature-dependent shift of most phonon modes in $BaTiO_3$ are suppressed upon Eu doping (the largest being for the *P5* mode ∼25 cm^{-1}). Moreover, the phonon modes in the tetragonal crystal structure disappear at a 40-K lower temperature in $Eu_{0.2}Ba_{0.8}TiO_3$ as compared to $BaTiO_3$. In addition, the jump in frequency across the structural transitions is not observed in *P3* and *P5*.

The difference in the temperature dependence (in all the phases) of the modes (Fig. 3) upon incorporating Eu^{2+} (by replacing Ba^{2+}) in $BaTiO_3$ could be due to the effect of (i) change in mass and (ii) change in lattice (local symmetries), both of which would lead to the changes in phonon anharmonicities. Replacement of lighter Ba^{2+} ions by heavier Eu^{2+} ions in $BaTiO_3$ would redshift the mode frequency (because $\omega \propto m^{1/2}$) if the Ba atom is involved in a vibration (all the modes involve Ba atoms except the *P6* mode at 308 cm^{-1}). On the other hand, the ionic radius of Eu^{2+} is lower than that of Ba^{2+} that shrinks the unit cell (at 300 K - $BaTiO_3$: $a = b = 3.9853$ Å, $c = 4.0069$ Å; $Eu_{0.2}Ba_{0.8}TiO_3$: $a = b = 3.9789$ Å, $c = 3.9982$ Å as shown in Figs. 1 and S2 [15]), which is expected to *blueshift* the mode frequencies. In other words, these two effects (change in mass and lattice) will compete and show a resultant effect on the mode frequencies and phonon anharmonicities. As can be seen in Fig. 3, all the modes show a clear *redshift* of frequency in $Eu_{0.2}Ba_{0.8}TiO_3$ as compared to that in $BaTiO_3$ except for *P4*, *P7*, *P9*, and *P10* wherein a noticeable *blueshift* can be observed. The temperature dependence of frequency of a phonon (i) may be expressed as [37–39]:

$$\omega^i(T) = \omega^i(0) + \Delta\omega^i_{qh}(T) + \Delta\omega^i_{anh}(T) + \Delta\omega^i_{el-ph} + \Delta\omega^i_{sp-ph}, \quad (1)$$

where $\omega^i(0)$ is the phonon frequency at 0 K. The term $\Delta\omega^i_{qh}(T)$ is the change in frequency due to the quasiharmonic contribution arising from the change in lattice volume (i.e., force constant) without changing the phonon population. The term $\Delta\omega^i_{anh}(T)$ is the change in frequency due to the intrinsic anharmonic contribution arising from the real part of the self-energy of a phonon decaying into two (cubic anharmonicity) or three (quartic anharmonicity) phonons. On the other hand, the terms $\Delta\omega^i_{el-ph}$ and $\Delta\omega^i_{sp-ph}$ are the changes in phonon frequency arising due to a coupling of the phonon with the charge carriers and spins, respectively, both of which are absent in these insulating and nonmagnetic materials ($BaTiO_3$ and $Eu_{0.2}Ba_{0.8}TiO_3$). Therefore, we can attribute the observed changes in phonon frequencies to the phonon anharmonicities.

Temperature-dependent changes in phonon anharmonicity are not only related to lattice volume but also to the phonon

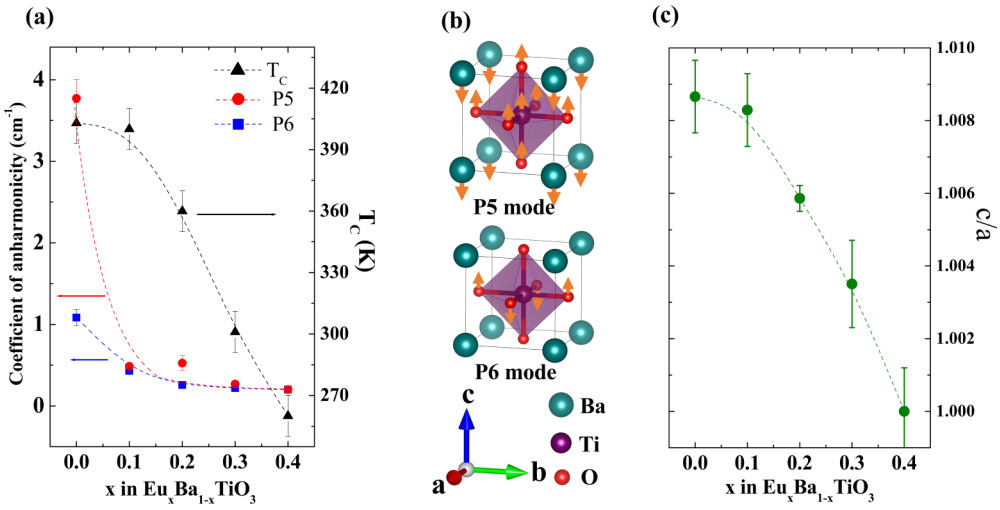

FIG. 4. (a) Dependence of the coefficient of phonon anharmonicity [as described in Eq. (2)] on the doping concentration of Eu^{2+} by replacing Ba^{2+} for the modes at 265 cm^{-1} (*P5*) and 308 cm^{-1} (*P6*). A decrease in phonon anharmonicity is evident with increasing Eu^{2+}. Similarly, the para-to-ferroelectric phase transition temperature (T_C) also decreases with increasing Eu^{2+}, as discussed in the main text. (b) Schematic of the atomic vibrations for the phonon modes at 265 cm^{-1} (*P5*) and 308 cm^{-1} (*P6*). (c) Reduction in tetragonality (ratio of *c* to *a* lattice parameters) of $Eu_xBa_{1-x}TiO_3$ at room temperature with increasing Eu^{2+}.The solid symbols in (a) and (c) represent the experimental data, while the dashed lines are guides to eye.

population (phonon density). In fact, phonon anharmonicities become significant when the temperature increases causing a phonon to decay into two or three phonons owing to cubic or quartic anharmonic interactions (or higher order interactions at much higher temperatures). Considering the three-phonon process (cubic anharmonicity), the temperature dependence of a phonon frequency (*i*) can be expressed as [39]

$$\omega^i(T) = \omega^i(0) + A\left[1 + \frac{2}{e^x - 1}\right], \qquad (2)$$

where $x = \hbar\omega^i(0)/2k_BT$, $\hbar$ is the reduced Planck's constant, k_B is the Boltzmann constant, T is the temperature, and A is the coefficient of anharmonicity. A comparison of Eqs. (1) and (2) indicates that the coefficient of anharmonicity A weighs the contributions of the quasiharmonic effect thus implicitly associating with the mode Grüneisen parameter and intrinsic anharmonic effects (see Sec. S5 in the Supplemental Material [15]). As mentioned earlier, the most surprising behavior is observed for the mode *P5* in $BaTiO_3$ (A_1 mode at 265cm^{-1}) that undergoes an unusually large change in frequency ~20 cm^{-1} over the temperature range of 300 to 400 K (see Fig. 3), indicating a strong phonon anharmonicity. Interestingly, upon replacing Ba^{2+} by Eu^{2+} the mode becomes nearly temperature independent, as shown in Fig 3. To understand this behavior of *P5*, we have quantified its phonon anharmonicity by fitting the frequency vs temperature using Eq. (2) (see Fig. S7 in the Supplemental Material [15]). As shown in Fig. 4(a), the mode *P5* has a very high coefficient of anharmonicity in pure $BaTiO_3$ which decreases with increasing doping of Eu^{2+}, clearly indicating a suppression of phonon anharmonicity (by ~ 93%) with increasing Eu^{2+}. The *P6* mode (B_1 at 308 cm^{-1}), which is present only in the ferroelectric phase also exhibits a similar decrease in anharmonicity (by ~73%) with increasing substitution of Ba^{2+} by Eu^{2+} [as shown in Fig. 4(a)]. It is important to note that the atomic displacements have an important role in phonon anharmonicity and the participating atoms in modes *P5* and *P6* displace along the crystallographic *c* axis, shown in Fig. 4(b), which decides the tetragonality of the lattice structure. The increase in atomic mass (due to the replacement of Ba^{2+} by Eu^{2+}) along with a decrease in the lattice constants (and unit cell volume as shown in Fig. S2 in the Supplemental Material [15]) with increasing Eu^{2+} should result in a reduced atomic displacement thus causing a decrease in the phonon anharmonicities. A detailed analysis of the quasiharmonic and intrinsic anharmonic contributions for all the phonon modes can be found in the Supplemental Material (Fig. S8) [15,40], which further elucidates that modes involving vibrations along the *c* axis are more anharmonic in nature. The temperature (T_C) above which the mode *P6* disappears is the crystallographic (tetragonal to cubic) transition temperature of $BaTiO_3$, also associated with the ferroelectric to paraelectric phase transition. A comparison of the temperature-dependent Raman spectra of $Eu_xBa_{1-x}TiO_3$ ($x = 0, 0.1, 0.2, 0.3, 0.4,$ and1) from Fig. 2, and Figs. S5 and S6 in Supplemental Material [15] can help determine this T_C. As shown in Fig. 4(a), the T_C decreases with increasing Eu^{2+} in $BaTiO_3$ [41], a behavior that is strikingly similar to the change in tetragonality (ratio of *c* to *a* lattice parameters) of the unit cell of $BaTiO_3$ with increasing Eu^{2+} as shown in Fig. 4(c). In fact, this similarity suggests that the reduction of ferroelectric order is clearly related to the suppression of phonon anharmonicity. Furthermore, the dielectric constant of $Eu_xBa_{1-x}TiO_3$ as a function of temperature, as shown in Fig. S9 in the Supplemental Material [15], also reveals a decrease in the T_C with increasing Eu^{2+} thus corroborating our results shown in Fig. 4. The decrease in phonon anharmonicity and the ferroelectric transition temperature (T_C) with Eu^{2+}-doping indicate that these parameters are coupled thus opening a route to tailor the functionalities of ferroelectric materials [3,4].

III. METHODS

Polycrystalline $BaTiO_3$ and $Eu_xBa_{1-x}TiO_3$ ($x = 0.1$, 0.2, 0.3, 0.4, and 1) powder samples were synthesized using a solid state reaction route where $BaCO_3$, TiO_2, and Eu_2O_3 at stoichiometric ratio were used as precursors [42]. The well mixed and ground powder for $BaTiO_3$ was calcined at 1200 ˚C for 24 h in air. However, the powder for $Eu_xBa_{1-x}TiO_3$ was calcined in reduced atmosphere (95%Ar-5%H_2) in order to reduce Eu^{3+} to Eu^{2+}. Two more cycles of grinding and heating at 1200 ˚C were done followed by which the powders were pelletized and sintered at 1300 ˚C for 24 h in the same atmosphere. The polycrystalline samples were characterized by x-ray diffraction at room temperature and found to be phase pure. Further, the x-ray diffraction patterns were measured using PANalytical Empyrean x-ray diffractometer (CuK_α line) as a function of temperature (Anton Paar TTK 450) from 90 to 450 K in order to probe the various structural phases and the corresponding lattice constants in $BaTiO_3$ and $Eu_{0.2}Ba_{0.8}TiO_3$. We would like to emphasize that based on our temperature-dependent x-ray diffraction measurements we have not been able to detect the presence of any impurity phase (of Eu^{3+}) within our experimental limit (see Sec. 1 in the Supplemental Material) [15,43–45]. However, it is to be noted that the low temperature sample stage (referred to as the LTStage) gives rise to additional reflection peaks in the range of 40˚–55˚ and near 75˚, which partially affects some of the $Eu_xBa_{1-x}TiO_3$ reflection peaks. The room temperature (300 K) data have been recorded on a different sample stage (referred to as the RTStage), which is free from those additional peaks and thus a comparison with the 300 K data allows us to identify the stage-related artefacts. The additional peaks from the LTStage have been partly removed for clarity. A detailed comparison of the LTStage x-ray diffraction patterns with those of $Eu_xBa_{1-x}TiO_3$ are given in the Supplemental Material (Sec. S1, Fig. S1) [15]. Further, magnetic measurements [42,46] of the powder samples of $Eu_xBa_{1-x}TiO_3$ suggest an almost pure Eu^{2+} state without any discernible impurity phase containing Eu^{3+} (see Fig. S3 and the discussion in the Supplemental Material [15]) thus confirming that the samples under study are in a highly pure phase.

The Raman spectra of $BaTiO_3$ and $Eu_xBa_{1-x}TiO_3$ were recorded in the backscattering geometry using a LabRAM HR Evolution Raman spectrometer equipped with a Peltier cooled charge coupled device detector. The samples were mounted on a liquid nitrogen cooled Linkam heating stage and excited with the 514.5-nm line of an Ar^+-ion laser with a typical power of ∼5mW on the sample. Further tests were also carried out using the 532-nm laser line of a frequency doubles Nd-YAG laser and the results were found to be similar.

IV. CONCLUSION

We have shown that phonon anharmonicities have an important association with ferroelectric ordering and the ferroelectric transition temperature in Eu^{2+}-doped $BaTiO_3$. Our experiments suggest that the competition between quantum fluctuations and ferroelectric ordering in $Eu_xBa_{1-x}TiO_3$ systems maintains a delicate balance with phonon anharmonicities, the suppression of which causes reduction of ferroelectric ordering. Tuning the phonon anharmonicity can therefore emerge as an additional route to tailor material functionalities that are coupled with the crystal structure.

ACKNOWLEDGMENTS

B.P. acknowledges the UGC, India, for fellowship. S. Sarkar acknowledges the NGS fellowship. R.M. acknowledges Ministry of Education, Singapore (Grant No. MOE2015-T2-2-147). T.V. acknowledges support from the National Research Foundation under Competitive Research Program (NRF2015NRF-CRP001-015). S.S. acknowledges SERB, India, for research grant (Project No. SERB/ECR/2016/001376) and financial support from DST-FIST [Project No. SR/FST/PSI-195/2014(C)]. The authors acknowledge M. Prajapat and A. Rathore at IISER Bhopal for their help during the x-ray diffraction measurements.

B.P., K.R., and S. Sarkar contributed equally to this work. B.P., S. Sarkar, and S.S. performed the Raman measurements and analyses. K.R. synthesized the samples under study and performed the dielectric and magnetic measurements. B.P performed the x-ray diffraction measurements. R.M., T.V., and S.S. planned and supervised the project. B.P., S. Sarkar, T.V., and S.S. wrote the manuscript with contributions from all the authors.

[1] K. M. Rabe, C. H. Ahn, and J.-M. Triscone, *Physics of Ferroelectrics: A Modern Perspective* (Springer, Berlin, 2007).

[2] F. Jona and G. Shirane, *Ferroelectric Crystals* (Pergamon Press, Oxford, 1962).

[3] T. Katsufuji and H. Takagi, Phys. Rev. B **64**, 054415 (2001).

[4] S. Kamba, D. Nuzhnyy, P. Vaněk, M. Savinov, K. Knížek, Z. Shen, E. Šantavá, K. Maca, M. Sadowski, and J. Petzelt, Europhys. Lett. **80**, 27002 (2007).

[5] T. R. McGuire, M. W. Shafer, R. J. Joenk, H. A. Alperin, and S. J. Pickart, J. Appl. Phys. **37**, 981 (1966).

[6] U. T. Höchli, K. Knorr, and A. Loidl, Adv. Phys. **39**, 405 (1990).

[7] V. V. Lemanov, E. P. Smirnova, P. P. Syrnikov, and E. A. Tarakanov, Phys. Rev. B **54**, 3151 (1996).

[8] M. E. Guzhva, V. V. Lemanov, P. A. Markovin, and W. Kleemann, Phys. Solid State **39**, 618 (1997).

[9] T. Wei, Q. J. Zhou, X. Yang, Q. G. Song, Z. P. Li, X. L. Qi, and J.-M. Liu, Appl. Surf. Sci. **258**, 4601 (2012).

[10] H. Wu, Q. Jiang, and W. Z. Shen, Phys. Rev. B **69**, 014104 (2004).

[11] V. Goian, S. Kamba, D. Nuzhnyy, P. Vaněk, M. Kempa, V. Bovtun, K. Knížek, J. Prokleška, F. Borodavka, M. Ledinský, and I. Gregora, J. Phys.: Condens. Matter **23**, 025904 (2011).

[12] A. O. Sushkov, S. Eckel, and S. K. Lamoreaux, Phys. Rev. A **81**, 022104 (2010).

[13] S. E. Rowley, L. J. Spalek, R. P. Smith, M. P. M. Dean, M. Itoh, J. F. Scott, G. G. Lonzarich, and S. S. Saxena, Nat. Phys. **10**, 367 (2014).

[14] M. Leroux, I. Errea, M. LeTacon, S. M. Souliou, G. Garbarino, L. Cario, A. Bosak, F. Mauri, M. Calandra, and P. Rodière, Phys. Rev. B **92**, 140303(R) (2015).

[15] See Supplemental Material at http://link.aps.org/supplemental/10.1103/PhysRevMaterials.3.024412 for additional data on x-ray diffraction, saturation magnetization, Raman spectroscopic, and dielectric constant measurements of $Eu_xBa_{1-x}TiO_3$ with relevant discussions. A detailed description of the Raman modes is also provided.

[16] G. H. Kwei, A. C. Lawson, and S. J. L. Billinge, J. Phys. Chem. **97**, 2368 (1993).

[17] Y. I. Yuzyuk, Phys. Solid State **54**, 1026 (2012).

[18] C. H. Perry and D. B. Hall, Phys. Rev. Lett. **15**, 700 (1965).

[19] G. Pezzottia, J. Appl. Phys. **113**, 211301 (2013).

[20] A. Pinczuk, W. Taylor, E. Burstein, and I. Lefkowitz, Solid State Commun. **5**, 429 (1967).

[21] L. Rimai, J. L. Parsons, and J. T. Hickmott, Phys. Rev. **168**, 623 (1968).

[22] J. D. Freire and R. S. Katiyar, Phys. Rev. B **37**, 2074 (1988).

[23] C. J. Xiao, Z. H. Chi, W. W. Zhang, F. Y. Li, S. M. Feng, C. Q. Jin, X. H. Wang, X. Y. Deng, and L. T. Li, J. Phys. Chem. Sol. **68**, 311 (2007).

[24] S. Rajan, P. M. M. Gazzali, and G. Chandrasekaran, J. Alloys Compd. **656**, 98 (2016).

[25] A. K. Sood, N. Chandrabhas, D. V. S. Muthu, and A. Jayaraman, Phys. Rev. B **51**, 8892 (1995).

[26] A. Chaves, R. S. Katiyar, and S. P. S. Porto, Phys. Rev. B **10**, 3522 (1974).

[27] H. Hayashi, T. Nakamura, and T. Ebina, J. Phys. Chem. Sol. **74**, 957 (2013).

[28] U. D. Venkateswaran, V. M. Naik, and R. Naik, Phys. Rev. B **58**, 14256 (1998).

[29] A. Scalabrin, A. S. Chaves, D. S. Shim, and S. S. P. Porto, Phys. Status Solidi B **79**, 731 (1977).

[30] C. M. Foster, Z. Li, M. Grimsditch, S.-K. Chan, and D. J. Lam, Phys. Rev. B **48**, 10160 (1993).

[31] C. M. Foster, M. Grimsditch, Z. Li, and V. G. Karpov, Phys. Rev. Lett. **71**, 1258 (1993).

[32] M. H. Frey and D. A. Payne, Phys. Rev. B **54**, 3158 (1996).

[33] Y. Shiratori, C. Pithan, J. Dornseiffer, and R. Waser, J. Raman Spectrosc. **38**, 1288 (2007).

[34] Z. Li, C. M. Foster, X.-H. Dai, X.-Z. Xu, S.-K. Chan, and D. J. Lam, J. Appl. Phys. **71**, 4481 (1992).

[35] G. Lucazeau, J. Raman Spectrosc. **34**, 478 (2003).

[36] M. Maczka, M. L. Sanjuán, A. F. Fuentes, K. Hermanowicz, and J. Hanuza, Phys. Rev. B **78**, 134420 (2008).

[37] S. Saha, S. Singh, B. Dkhil, S. Dhar, R. Suryanarayanan, G. Dhalenne, A. Revcolevschi, and A. K. Sood, Phys. Rev. B **78**, 214102 (2008).

[38] S. Saha, D. V. S. Muthu, S. Singh, B. Dkhil, R. Suryanarayanan, G. Dhalenne, H. K. Poswal, S. Karmakar, S. M. Sharma, A. Revcolevschi, and A. K. Sood, Phys. Rev. B **79**, 134112 (2009).

[39] M. Balkanski, R. F. Wallis, and E. Haro, Phys. Rev. B **28**, 1928 (1983).

[40] J. J. Wang, F. Y. Meng, X. Q. Ma, M. X. Xu, and L. Q. Chen, J. Appl. Phys. **108**, 034107 (2010).

[41] K. Rubi and R. Mahendiran, *IEEE International Magnetics Conference (INTERMAG) Proceedings* (IEEE, 2018), p. 18196407.

[42] K. Rubi, P. Kumar, D. V. M. Repaka, R. Chen, J.-S. Wang, and R. Mahendiran, Appl. Phys. Lett. **104**, 032407 (2014).

[43] D.-Y. Lu, T. Ogata, H. Unuma, X.-C. Li, N.-N. Li, and X.-Y. Sun, Solid State Ionics **201**, 6 (2011).

[44] J. H. Van Vleck and A. Frank, Phys. Rev. **34**, 1494 (1929); **34**, 1625 (1929).

[45] M. Barbagallo, T. Stollenwerk, J. Kroha, N.-J. Steinke, N. D. M. Hine, J. F. K. Cooper, C. H. W. Barnes, A. Ionescu, P. M. D. S. Monteiro, J.-Y. Kim, K. R. A. Ziebeck, C. J. Kinane, R. M. Dalgliesh, T. R. Charlton, and S. Langridge, Phys. Rev. B **84**, 075219 (2011).

[46] A. Midya, P. Mandal, K. Rubi, R. Chen, J.-S. Wang, R. Mahendiran, G. Lorusso, and M. Evangelisti, Phys. Rev. B **93**, 094422 (2016).